Effects of sea ice cover on acoustic ray travel times, with applications to the Greenland Sea tomography experiment

Guoliang Jin
Shanghai Acoustics Laboratory, Academia Sinica, Shanghai 200032, People's Republic of China

J. F. Lynch and R. Pawlowicz
Woods Hole Oceanographic Institution, Woods Hole, Massachusetts 02543

P. Wadhams
Scott Polar Research Institute, University of Cambridge, Lensfield Road, Cambridge CB2 1ER, United Kingdom

(Received 3 August 1992; revised 11 February 1993; accepted 18 February 1993)

The travel-time effects of a sea ice cover on an acoustic pulse are estimated using generalized ray theory. This expands upon the previous work done by Jin and Wadhams [Prog. Oceanogr. **22**, 249–275 (1989)] by including the effects of frequency dispersion and different sets of ice parameters. Travel-time changes due to single reflections are approximated by plane wave reflection theory, and compared to the generalized ray theory results. Statistical effects for multiple reflections, such as the ice thickness probability distribution function, Fresnel zone averaging, and shadowing are considered. Finally, the effects of ice-induced travel-time changes on tomographic inversions for water column oceanography are considered. The implications of this work on the 1988–89 Greenland Sea tomography experiment are considered in detail.

PACS numbers: 43.30.Cq, 43.30.Pc, 43.30.Ma

INTRODUCTION

Ocean acoustic tomography is an oceanographic measurement technique for monitoring the large-scale sound speed (temperature) and current structure of the ocean by carefully measuring acoustic pulse travel times between the elements of a source/receiver array.[1] Travel-time signatures of ocean features are typically of order 10–100 ms for temperature and 0–20 ms for currents. In order to measure the ocean well, errors in the travel time, both random and systematic, must be less than the signals from the ocean. Clock accuracies in tomographic systems are designed to be of order 1 ms per year to avoid confusion of clock drift with ocean signals. Mooring motion is generally monitored to within a meter, corresponding to less than a millisecond timing error. Unwanted oceanographic signals, e.g., tides and internal waves if one is looking at eddies, also contribute to travel-time error, and are filtered out where possible.

When tomography was first conceived, energy interacting with the ocean boundaries was assumed to be "lost" due to the effects of scattering. However, during the decade or so of experimental work in tomography that has followed the 1981 "demonstration experiment,"[2] energy interacting with the boundaries, both bottom and surface, was found to be both experimentally usable (i.e., stable, resolvable, and identifiable rays were routinely seen) and in fact quite valuable.[3–5] Recently, a number of efforts have been made to understand the travel-time effects of surface scattering. Lynch *et al.*,[6] have shown, in the context of adiabatic normal mode theory, that the scattering of acoustic energy by surface gravity waves results in negligible wander and bias of the arrivals received in a standard tomography experiment, i.e., small fractions of a millisecond. Prompted by the Greenland Sea tomography experiment,[7] which took place between September 1988 and September 1989, a number of researchers began to look at what the travel-time effects of sea ice would be. In his Ph.D. thesis, Romm[8] considered the effects of very thin ice layers in terms of normal mode theory. Jin and Wadhams[9] studied realistic ice cover effects on the basis of ray theory by estimating the beam displacement and time delay at reflections from the ice water interface, though ignoring the effects of frequency dispersion.

In this paper, generalized ray theory methods are used to investigate the effects of ice cover on the travel time. Frequency dispersion, which may cause considerable distortion of the received pulse shapes, is explicitly taken into account. The effects of different sets of ice parameters, including relatively low shear speeds (typifying unconsolidated keels, for instance) are also examined. Single reflections from the ice are considered in both the plane wave and generalized ray approximations. Statistical methods are developed to deal with realistic sea ice cover effects, such as partial ice cover and regionally varying ice properties. Acoustic ray interactions with rough surfaces also include Fresnel zone size and shadowing effects, which are considered. Finally, we apply our results to estimating the travel-time effects of ice upon the sound-speed inversions performed for the Greenland Sea tomography experiment.

I. GENERALIZED RAY EXPRESSIONS FOR AN ACOUSTIC PULSE

In Arctic regions, the water column is to first order isothermal and near the freezing point. This is especially the case in the uppermost 200-m underneath ice cover. Thus the sound speed versus depth is controlled by the hydrostatic pressure term in the equation of state, salinity

 0001-4966/93/94(2)/1044/14/$6.00

effects being of second order. This leads to profiles with positive (nearly) linear gradients and a duct right at the surface. In this paper, we will restrict ourselves to this simple case. Generalizations of our work to more complicated profiles is, for the most part, trivial.

By making a multipath expansion of the reduced-wave equation and using WKB solutions of the depth-dependent wave equation, the acoustic pressure due to a point harmonic source can be expressed as[10,11]

$$p(r,z,z_0,\omega)=\sum_{n=0}^{\infty}\sum_{m=1}^{4}p_n^{(m)}(r,z,z_0,\omega), \tag{1}$$

where z_0 and z are, respectively, the source and receiver depths, n is the number of surface reflections, r is the range, ω is the angular frequency and

$$p_n^{(m)}=\int_{-\infty}^{k(z)}K_n^{(m)}(r,z,z_0,\mu)\exp[i\xi_n^{(m)}(r,z,z_0,\mu)]d\mu, \tag{2}$$

where $k(z)$ is the wave number, μ is the horizontal wave number,

$$K_n^{(m)}=|V_s|^n\sqrt{\frac{\mu}{2\pi rq(z)q(z_0)}}\,e^{-i(3/4)\pi}\begin{cases}1, & m=1 \text{ or } 3,\\ |V_s|, & m=2 \text{ or } 4,\end{cases} \tag{3}$$

$$q(z)=\sqrt{k^2(z)-\mu^2}, \tag{4}$$

and

$$\begin{aligned}
\xi_n^{(1)}&=\int_z^{z_0}q\,dz+2n\int_0^{z_t}q\,dz+n\phi_s-\frac{n\pi}{2}+\mu r,\\
\xi_n^{(2)}&=\int_0^{z_0}q\,dz+\int_0^{z}q\,dz+2n\int_0^{z_t}q\,dz+(n+1)\phi_s\\
&\quad-\frac{n\pi}{2}+\mu r,\\
\xi_n^{(3)}&=\int_z^{z_t}q\,dz+\int_{z_0}^{z_t}q\,dz+2n\int_0^{z_t}q\,dz\\
&\quad+n\phi_s-\frac{(n+1)\pi}{2}+\mu r,\\
\xi_n^{(4)}&=2\int_0^{z_t}q(z)dz-\int_z^{z_0}q\,dz+2n\int_0^{z_t}q\,dz+(n+1)\phi_s\\
&\quad-\frac{(n+1)\pi}{2}+\mu r.
\end{aligned} \tag{5}$$

Here, V_s is the surface reflection coefficient, $\phi_s=\arg(V_s)$, and z_t is the depth of ray turning point.

Equation (2) can be approximated using the method of stationary phase. The stationary phase point $\mu_n(r,z,z_0)$ is found from the equation

$$\left(\frac{\partial\xi_n^{(m)}}{\partial\mu}\right)_{\mu_n}=0. \tag{6}$$

Substituting (5) into (6) yields

$$\begin{aligned}
m=1,\quad & r=\int_z^{z_0}B_n\,dz+2n\int_0^{z_t}B_n\,dz-\frac{n\pi}{2}+n\delta_s(\mu_n),\\
m=2,\quad & r=\int_0^{z}B_n\,dz+\int_0^{z_0}B_n\,dz+2n\int_0^{z_t}B_n\,dz-\frac{n\pi}{2}\\
&\quad+(n+1)\delta_s(\mu_n),\\
m=3,\quad & r=\int_z^{z_t}B_n\,dz+\int_{z_0}^{z_t}B_n\,dz+2n\int_0^{z_t}B_n\,dz\\
&\quad-\frac{(n+1)\pi}{2}+n\delta_s(\mu_n),\\
m=4,\quad & r=2\int_0^{z_t}B_n\,dz-\int_z^{z_0}B_n\,dz+2n\int_0^{z_t}B_n\,dz\\
&\quad-\frac{(n+1)\pi}{2}+(n+1)\delta_s(\mu_n),
\end{aligned} \tag{7}$$

where

$$B_n\equiv\frac{\mu_n}{\sqrt{k^2-\mu_n^2}} \tag{8a}$$

and

$$\delta_s=-\left(\frac{\partial\phi_s}{\partial\mu}\right)_{\mu_n} \tag{8b}$$

is the beam displacement at points of surface reflection.[12] Let $\mu_n\equiv k(z)\cos\theta_n(z)$. Then the equation for the stationary point (7) is just the ray equation for grazing angle $\theta_n(z)$.

For noncaustic regions, i.e., $(\partial^2\xi_n^{(m)}/\partial\mu^2)_{\mu_n}\neq 0$, we can expand $\xi_n^{(m)}$ at the point of stationary phase, and the sound pressure can be expressed as

$$\begin{aligned}
p(r,z,z_0,\omega)=&\sum_{n=0}^{\infty}\sum_{m=1}^{4}A_n^{(m)}(r,z,z_0,\mu_n)\\
&\times\exp[i\Phi_n^{(m)}(r,z,z_0,\mu)],
\end{aligned} \tag{9}$$

where

$$\begin{aligned}
A_n^{(m)}=&|V_s|^n\left[r\left(\frac{\partial r}{\partial\theta_n(z_0)}\right)\tan\theta_n(z)\right]^{-1/2}e^{-i(\pi/2)}\\
&\times\begin{cases}1, & m=1 \text{ or } 3,\\ |V_s|, & m=2 \text{ or } 4,\end{cases}
\end{aligned} \tag{10}$$

and $\Phi_n^{(m)}=\xi_n^{(m)}(r,z,z_0,\mu_n)$. That is, $\Phi_n^{(m)}$ is determined from Eq. (5) by replacing μ by μ_n.

Let us now consider the expression of pulse fields. The relation between the waveform of transmitted sound pulse $s_0(t)$ and its frequency spectrum $g(\omega)$ is given by the Fourier transform pair:

$$\begin{aligned}
S_0(t)&=\frac{1}{2\pi}\int_{-\infty}^{\infty}e^{-i\omega t}g(\omega)dw,\\
g(\omega)&=\int_{-\infty}^{\infty}e^{i\omega t}S_0(t)dt.
\end{aligned} \tag{11}$$

The pulse field at (r,z) can be expressed as

$$S(r,z,z_0,t)=\frac{1}{2\pi}\int_{-\infty}^{\infty} g(\omega)p(r,z,z_0,\mu_n,\omega)e^{-i\omega t}\,d\omega$$

$$=\int_{-\infty}^{\infty}\frac{1}{2\pi}g(\omega)\Bigg(\sum_{n=0}^{\infty}\sum_{m=1}^{4}A_n^{(m)}\times(r,z,z_0,\mu_n,\omega)\exp i[\Phi_n^{(m)}\times(r,z,z_0,\mu_n,\omega)-\omega t]\Bigg)d\omega. \tag{12}$$

Using the above equation, we can calculate the received signal waveforms and their travel times.

By exchanging the order of integration and summation in (12), we obtain

$$S(r,z,z_0,t)=\sum_{n=0}^{\infty}\sum_{m=1}^{4}S_n^{(m)}(r,z,z_0,t), \tag{13}$$

where

$$S_n^{(m)}=\frac{1}{2\pi}\int_{-\infty}^{\infty}g(\omega)A_n^{(m)}(r,z,z_0,\mu_n,\omega)\times\exp\{-i[\Phi_n^{(m)}(r,z,z_0,\mu_n,\omega)-\omega t]\}d\omega. \tag{14}$$

Here, $S_n^{(m)}$ is called a "generalized ray pulse."

For a narrow-band pulse of width $2\Delta w$ with the central frequency ω_0, we may expand $\Phi_n^{(m)}(\omega)$ in a series in powers of $(\omega-\omega_0)$ to obtain

$$\Phi_n^{(m)}(\omega)=\Phi_n^{(m)}(\omega_0)+\left(\frac{\partial\Phi_n}{\partial\omega}\right)_{\omega_0}(\omega-\omega_0)+\frac{1}{2}\left(\frac{\partial^2\Phi_n}{\partial\omega^2}\right)_{\omega_0}(\omega-\omega_0)^2+\cdots. \tag{15}$$

If

$$\frac{1}{2}\left|\left(\frac{\partial^2\Phi_n}{\partial\omega^2}\right)_{\omega_0}\right|(\omega-\omega_0)^2\leqslant\frac{1}{2}\left|\left(\frac{\partial^2\Phi_n}{\partial\omega^2}\right)_{\omega_0}\right|(\Delta\omega)^2\ll 1, \tag{16}$$

then

$$\Phi_n^{(m)}(\omega)\approx\Phi_n^{(m)}(\omega_0)+\left(\frac{\partial\Phi_n}{\partial\omega}\right)_{\omega_0}(\omega-\omega_0). \tag{17}$$

Substituting Eq. (17) into Eq. (14) yields

$$S_n^{(m)}\approx A_n^{(m)}(\omega_0)\exp i\left[\Phi_n^{(m)}(\omega_0)-\left(\frac{\partial\Phi}{\partial\omega}\right)_{\omega_0}\omega_0\right]\times S_0\left[t-\left(\frac{\partial\Phi_n}{\partial\omega}\right)_{\omega_0}\right]. \tag{18}$$

This means that the pulse shape remains the same during the propagation and the travel time is given by

$$T_n^{(m)}=\left(\frac{\partial\Phi_n}{\partial\omega}\right)_{\omega_0}. \tag{19}$$

From Eq. (5) we have

$$T_n^{(1)}(\mu_n)=\int_z^{z_0}D_n\,dz+2n\int_0^{z_t}D_n\,dz+n\tau_s(\mu_n,\omega_0),$$

$$T_n^{(2)}(\mu_n)=\int_0^{z_0}D_n\,dz+\int_0^{z}D_n\,dz+2n\int_0^{z_t}D_n\,dz+(n+1)\tau_s(\mu_n,\omega_0),$$

$$T_n^{(3)}(\mu_n)=\int_z^{z_t}D_n\,dz+\int_{z_0}^{z_t}D_n\,dz+2n\int_0^{z_t}D_n\,dz+n\tau_s(\mu_n,\omega_0), \tag{20}$$

$$T_n^{(4)}(\mu_n)=2\int_0^{z_t}D_n\,dz-\int_z^{z_0}D_n\,dz+2n\int_0^{z_t}D_n\,dz+(n+1)\tau_s(\mu_n,\omega_0),$$

where

$$D_n\equiv k/c\sqrt{k^2-\mu_n^2}$$

and

$$\tau_s(\mu_n,\omega_0)=\left(\frac{\partial\phi_s(\mu_n,\omega)}{\partial\omega}\right)_{\omega=\omega_0} \tag{21}$$

is the time delay due to the surface reflection.

When the frequency dispersion due to the reflection can be neglected, i.e., when the inequality Eq. (16) is satisfied, Eq. (20) can be used for estimating the pulse arrival time as was done in the earlier paper by Jin and Wadhams.

II. TRAVEL-TIME CHANGES DUE TO AN ICE COVER OF UNIFORM THICKNESS

When there is ice cover, reflections occur from the ice–water interface instead of the free surface. Hence the reflection coefficient and the depth level at which the reflections occur are both changed. These changes both affect the travel time.

According to Brekhovskikh[12] the reflection coefficient of a plane wave at the ice–water interface is given by

$$V_s=\frac{-(MZ_1)Z_3+i[(MZ_1)^2-(NZ_1)^2]}{(MZ_1)Z_3+i[(MZ_1)^2-(NZ_1)^2]}, \tag{22}$$

where

$$MZ_1=Z_2\cos^2 2\gamma_2\cot p+Z_{2t}\sin^2 2\gamma_2\cot Q,$$

$$NZ_1=Z_2\cos^2 2\gamma_2/\sin p+Z_{2t}\sin^2 2\gamma_2/\sin Q,$$

$$Z_2=\rho_2c_2/\cos\theta_2,\quad Z_{2t}=\rho_2b_2/\cos\gamma_2,$$

$$Z_3=\rho_3c_3/\cos\theta_3,$$

$$p=k_2h\cos\theta_2,\quad Q=K_2h\cos\gamma_2,$$

$$\frac{\sin\theta_3}{c_3}=\frac{\sin\gamma_2}{b_2}=\frac{\sin\theta_2}{c_2},$$

$$k_2=\omega/c_2,\quad K_2=\omega/b_2.$$

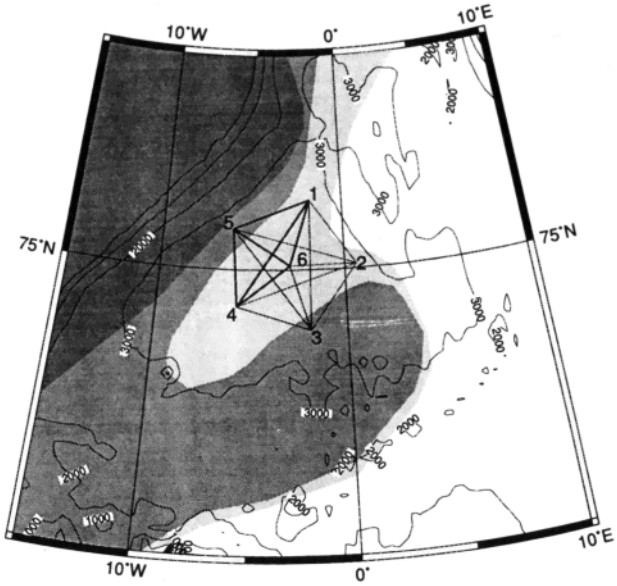

FIG. 1. Mooring array configuration (GSP88 array) for the Greenland Sea tomography experiment. Darkest shaded area in September ice cover, next darkest is March ice cover, and lightest is December ice cover.

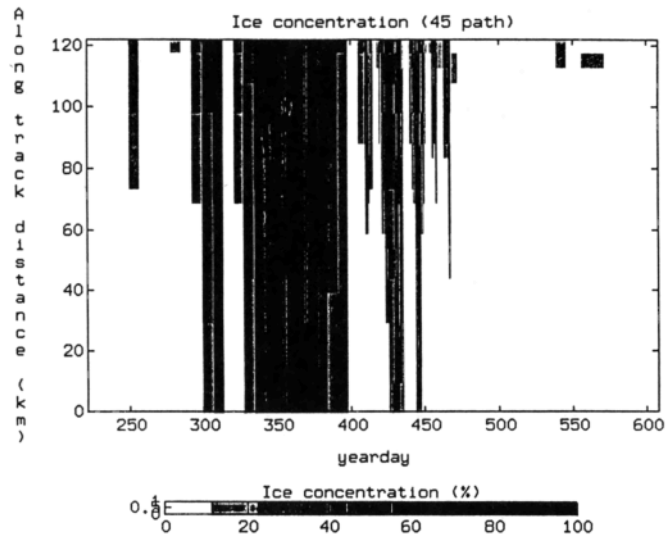

FIG. 2. Ice cover (concentration) between moorings 4 and 5 during the Greenland Sea tomography experiment.

Here ρ, c, b are the (constant) density, compressional wave and shear wave velocities in the media. The subscripts 2 and 3 denote the ice layer and sea water, respectively, h is the ice thickness, θ_3 is the incident angle, and θ_2 and γ_2 are the refraction angles for compressional and shear waves, respectively, in the ice layer.

When we consider the sound absorption which exists in the ice layer, M, N, Z_2, and Z_{2f} are all complex. For our studies we have employed the following relations for the compressional and shear wave absorption coefficients, α and β (Ref. 13):

$$\alpha=\alpha_0 f \quad (\text{dB/m}), \quad \beta=6\alpha \quad (\text{dB/m}), \tag{23}$$

where f is the frequency in kHz and α_0 is determined from the absorption at 1 kHz.

We have used the generalized ray method [Eq. (12)] to calculate the received pulse waveforms and travel-time changes caused by ice covers of different ice thicknesses and physical properties. In our calculations, the pulse arrival time is determined by the centroid of the arriving pulse.

As a calculation example, which is also of great practical interest to us, we will consider the propagation and scattering for the geometry and environmental conditions specific to the two westernmost moorings deployed during the Greenland Sea tomography experiment. These moorings, which are denoted by 4 and 5 in Fig. 1, also experienced the highest degree of ice cover between them, which is shown in Fig. 2. The appropriate environmental and experimental geometry quantities were

source depth	94.6 m,
receiver depth	101.5 m,
receiver range	121.947 km,
water depth (avg.)	3400 m,
ice density	0.91 g/cm^3,
source central frequency	250 Hz,
frequency bandwidth	125 Hz,
sound velocity in sea water	$c(z)=1443.16+0.01728z$ (m/s).

The compressional and shear velocities, c_2 and b_2, of sea ice vary with temperature, salinity, and ice history. Many different ranges of sea ice sound velocities have been reported.[14–16] Compressional wave velocities may lie between 2100 and 3800 m/s and shear wave velocities can range from 1100 to 1850 m/s. The compressional and shear wave absorption coefficients of sea ice are also temperature dependent. In our calculations four sets of ice parameters, shown in Table I, were used to cover the broad range of possible parameters. A homogeneous ice layer was assumed for simplicity even though, in general, ice has a layered structure. We tacitly assume that the longer wavelengths we used tend to average out the smaller details of ice structure.

The arrival pattern between moorings 4 and 5 of the first 16 rays in the absence of ice cover is shown in Fig. 3, where there are four ray groups. In each ray group, the individual ray grazing angles at the ice–water interface are very close, and given the system bandwidth we used, the

TABLE I. Material parameters for four different ice types.

	C_c (m/s)	C_s (m/s)	α_0 (dB/mkHz)	
case 1	3500	1800	0.06	winter/spring ice in Arctic Ocean[8,14]
case 2	3000	1600	0.06	summer ice in central Arctic Ocean[14]
case 3	3650	1450	0.198	summer Greenland Sea MIZ[15]
case 4	2700	1100	0.198	young sea ice ridges[16]

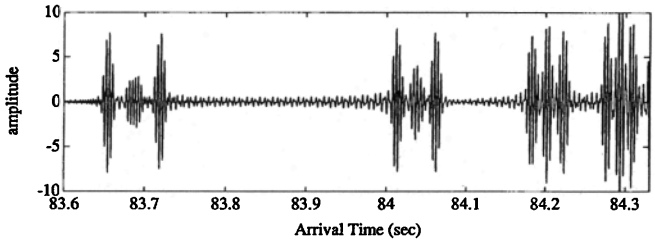

FIG. 3. The arrival pattern of the first four ray groups in the absence of ice cover.

TABLE II. Ray path parameters.

Ray path	1	4	5	8	9	12	13	16
grazing angle (degrees)	13.7	13.6	10.4	10.3	8.3	8.2	7.0	6.8
number of surface reflections	2	4	3	5	4	6	5	7

first and the last ray arrivals in each group are time separable whereas the middle two arrivals are not resolvable. The parameters of ray paths 1, 5, 9, 13 (the first arrivals in each group) and 4, 8, 12, 16 (the last arrivals in each group) are given in Table II.

Figure 4 shows the calculated arrival waveforms of the first (13°) ray group at ice thickness of 0, 1, 2, and 3 m for the four ice cases in Table I. For cases 1 and 2 the ice shear velocities are relatively high and the reflections at ice–water interface are total internal ones. Therefore the distortion of the pulse shapes is small. For cases 3 and 4, the ice shear velocities are low and sound waves can penetrate into the ice. Multiple reflection from the ice–air and ice–water interfaces can occur, resulting in considerable waveform distortions and travel time changes, especially at resonant thicknesses. As is well known, sound waves can propagate through the ice in modes corresponding to the Lamb modes, which take energy away from the incident beam. In this case, reflection loss increases where reso-

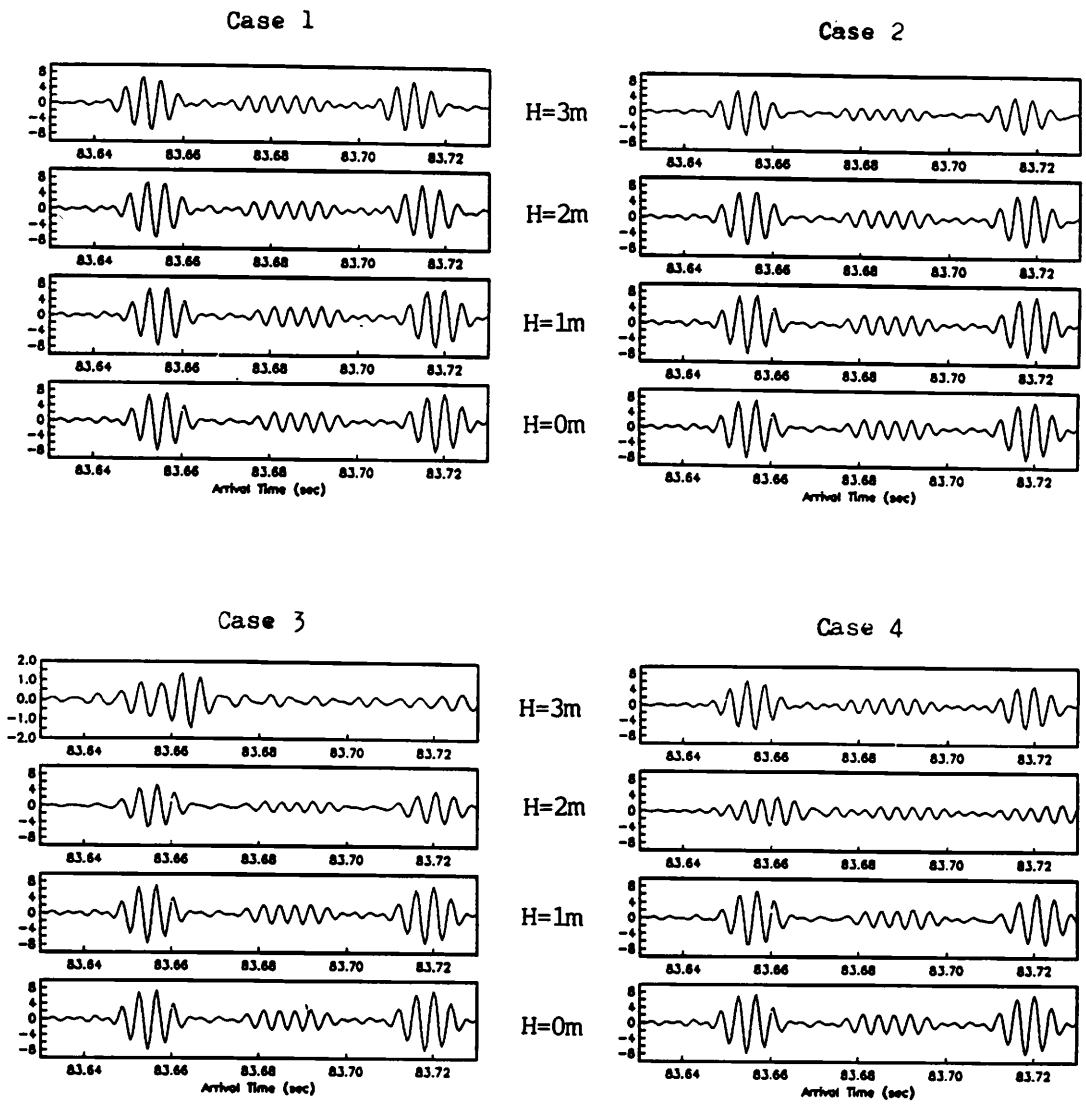

FIG. 4. Arrival patterns of the first ray group at ice thicknesses 0, 1, 2, and 3 m for the four ice cases.

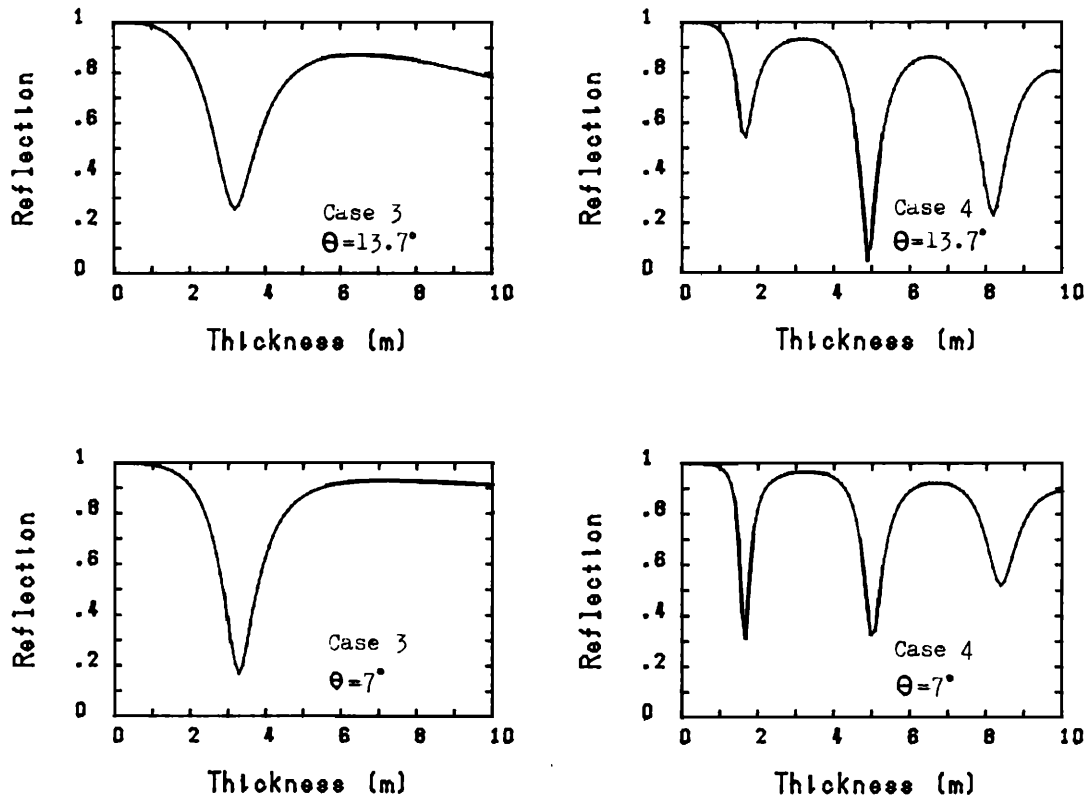

FIG. 5. Modulus of reflection coefficient for grazing angles 13.7° and 7° at a frequency of 250 Hz versus ice thickness for ice cases 3 and 4.

nance occurs. This can be seen from Fig. 5, which shows the modulus of the reflection coefficient as a function of the ice thickness at frequency 250 Hz for cases 3 and 4. The calculated travel-time changes of rays 4, 8, 12, and 16 for the four ice parameter cases are given in Fig. 6, where positive values correspond to decrease of travel time. The travel-time retardation at the resonant thicknesses are clearly seen.

III. TRAVEL-TIME CHANGES CAUSED BY A SINGLE REFLECTION

In the above section we estimated the travel-time changes by considering pulse propagation along the whole ray path. We now ask: Is it possible to estimate the total travel-time changes by adding the effects of individual reflections at the ice–water interface? Let us consider first the travel-time change due to a single reflection. As mentioned before, in the presence of an ice cover, the reflection coefficient, and the depth level at which the reflection occurs are both changed. These changes affect the travel time and the two effects can be considered separately.[9]

Under the plane wave approximation the travel-time change due to the depth level change for a single reflection (ice draft effect) can be expressed as

$$\Delta T_d=(2D/c)\sin\theta, \tag{24}$$

where D is the ice draft, θ is the ray grazing angle at the surface, and c is the sound speed of sea water near the surface.

When the frequency dispersion at reflection can be neglected, the travel-time change due to the change of the reflection coefficient (from a free surface to an ice–water interface) for a single reflection under the plane wave approximation can be expressed as

$$\Delta T_h=\delta_s\cos\theta/c-\tau_s, \tag{25}$$

where δ_s and τ_s are, respectively, the beam displacement and the time delay at the reflection, given by Eqs. (8) and (21). Therefore the total travel-time change produced by a single reflection is

$$\Delta T=\Delta T_d+\Delta T_h. \tag{26}$$

When the frequency dispersion or waveform distortion cannot be ignored, ΔT_h should be estimated in terms of the generalized ray method for a single reflection. In this case the sea water can be assumed to be homogenous (isovelocity), and the source and receiver positions are assigned to get the required ray grazing angle θ at the surface.

Now let us consider the possibility of estimating the travel-time change for a certain ray path by adding the time changes due to individual reflections, that is,

$$\Delta T_{\text{ray}}=\sum_{i=1}^{N}\Delta T_i, \tag{27}$$

where N is the number of surface reflection and ΔT_i is the time changes due to individual reflections given by (26). By assuming an ice cover of uniform thickness, Eq. (27) becomes

$$\Delta T_{\text{ray}}=N\,\Delta T. \tag{28}$$

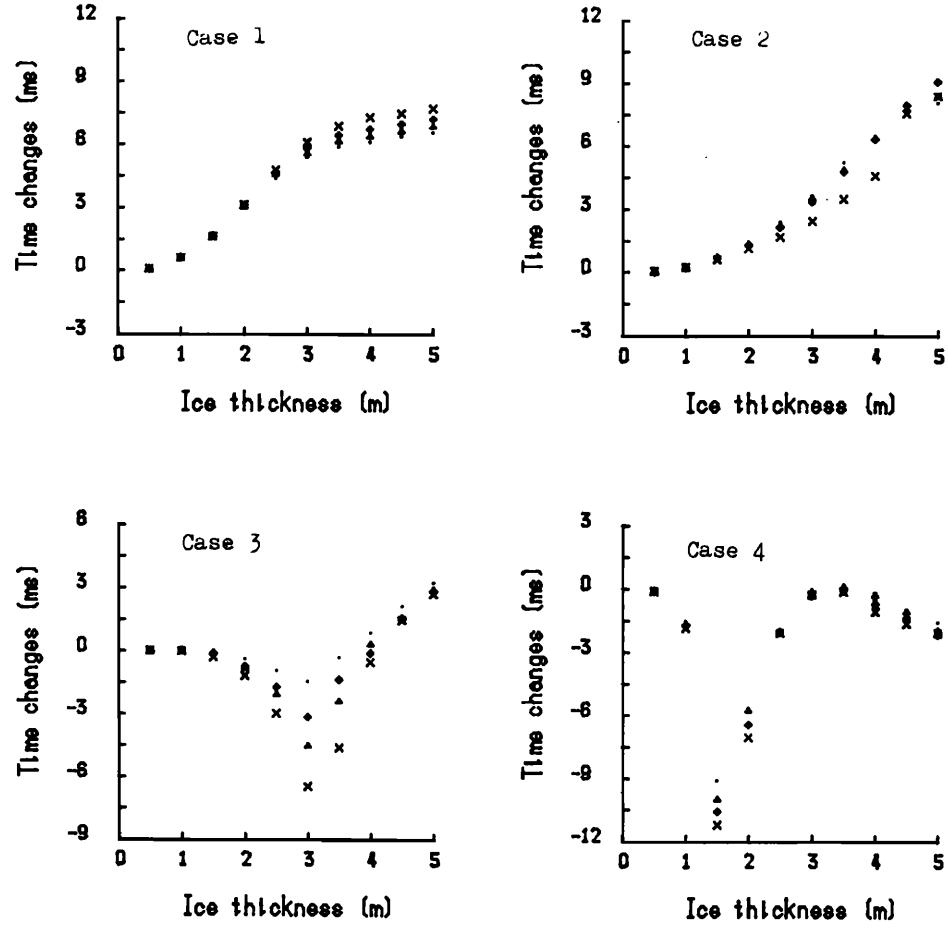

FIG. 6. Calculated travel-time changes of rays 4, 8, 12, and 16 versus ice thickness for the four ice cases. ×—ray 4, ◇—ray 8, △—ray 12, ●—ray 16.

As examples, Figs. 7 and 8 show the travel-time changes of rays 1 and 13 for the four ice parameter cases, calculated in terms of three different methods. Method 1 is rigorous, i.e., the generalized ray method was used to calculate the travel-time changes along the ray paths as we did in Sec. II. Both methods 2 and 3 calculated travel-time changes by adding the time changes due to individual reflections [Eq. (28)]. In estimating ΔT_h method 2 used the generalized ray method, whereas method 3 used Eq. (25) which ignores frequency dispersion. In Fig. 7, we see that the results of the three methods are very close. This means that the errors induced by the approximation of adding time changes due to individual reflections while ignoring frequency dispersion are small for ice cases 1 and 2. In these cases, the shear velocities are relatively high resulting in total internal reflection to the ice–water interface. From Fig. 8 it is clear that for relatively low shear velocities (ice cases 3 and 4) method 3 may induce considerable errors, especially in the resonant region, demonstrating that the frequency dispersion sometimes cannot be ignored. Errors for method 2 are still small for ray 1 ($N=2$), but may be considerable for ray 13 ($N=5$) in the resonant region. Looking at Eq. (14), we remember that the travel-time change is also related to the frequency spectrum of pulse. Since the pulse shape (frequency spectrum) is distorted by resonant reflections, the time changes of individual reflections may be considerably different for a succession of reflections, especially for large numbers of reflection. Therefore, large errors may be induced by using Eq. (28) for a succession of resonant reflections.

IV. STATISTICAL CONSIDERATIONS

Sea ice is composed of leads and pressure ridges as well as undeformed ice, and the ice thickness is nonuniform. Because of these complexities, the approximate expression (27) needs to be used. The travel-time changes of individual reflections should be estimated (using our methods) by using the local ice thickness along with the assumption of a locally flat subice interface. Furthermore, if the probability distribution function of ice thickness PDF (h,r) is known, the travel-time changes can be estimated in a statistical way:

$$\Delta T = \sum_{i}^{N} \int_{0}^{\infty} \tau(h)\mathrm{PDF}(h,r_i)dh, \tag{29}$$

where $\tau(h)$ is the travel time changes as a function of ice thickness for a single reflection, and r_i is the range for ith reflection. Given the frequency spectrum of the pulse, the ray grazing angle at the surface, the ice compressional and shear velocities and absorption coefficients, $\tau(h)$ can be calculated in terms of the generalized ray methods or more simply from Eq. (25) ignoring frequency dispersion. For

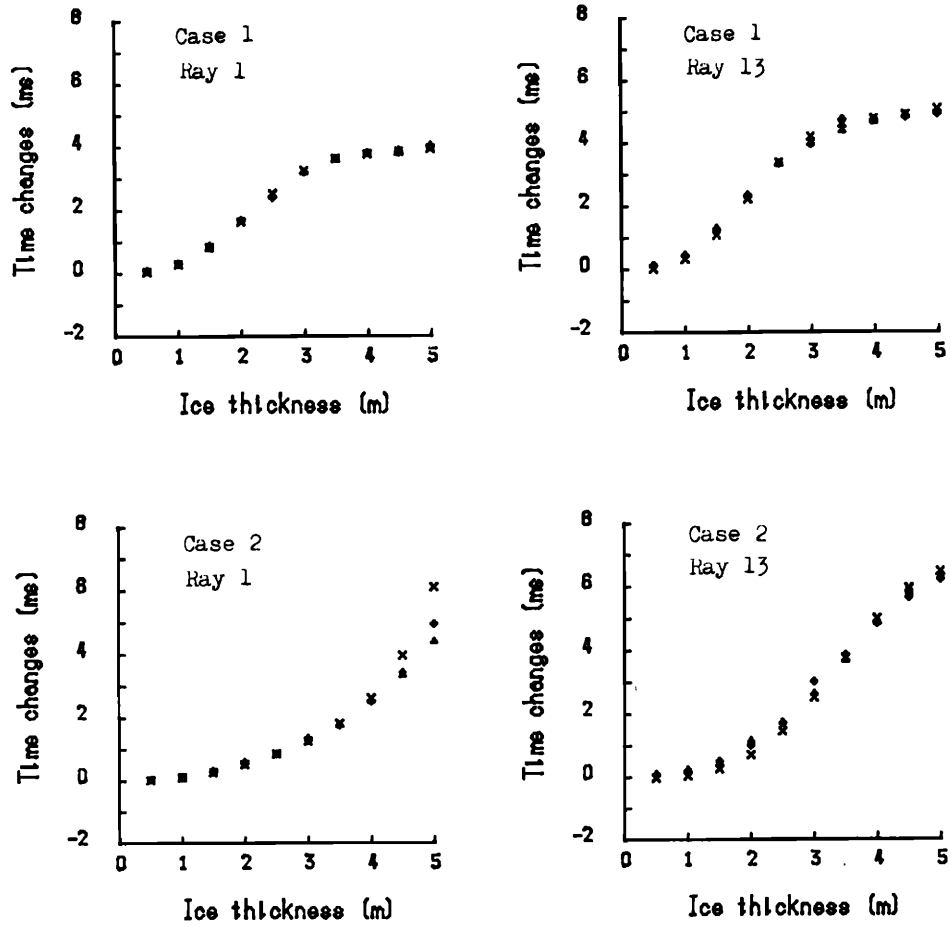

FIG. 7. Calculated travel-time changes of rays 1 and 13 for ice cases 1 and 2 in terms of the three methods. △—method 1, ◇—method 2, ×—method 3.

partial ice cover the probability of zero ice thickness should be included in the PDF.

For a range-independent PDF, Eq. (29) becomes

$$\Delta T = N \int_0^\infty \tau(h)\mathrm{PDF}(h)dh. \tag{30}$$

Figure 9 shows two probability density functions of ice draft obtained by British submarines in the Greenland Sea marginal ice zone in May 1987 and July 1985.[17,18] The mean values are 1.6 and 2.9 m, respectively, for PDF 1 and PDF 2. We took the two PDF's as examples to calculate the travel-time change in terms of Eq. (30). Functions $\tau(h)$ were calculated for the four ice parameter cases at grazing angles of 13.7° and 7° using the generalized ray method. Table III give the estimated travel-time changes Δt and standard deviations σ for rays 1, 4, 13, and 16. If needed, the function $\tau(h)$ can also be calculated using thickness-dependent ice parameters.

The absorption coefficient may also play an important role in the resonant region. Figure 10 shows the calculated $\tau(h)$ at $\theta=7°$ for ice cases 1 and 4 using different absorption coefficients. For case 1 the results for the two different absorptions are almost the same. However for case 4 functions $\tau(h)$ are considerably different. This is because bigger absorption results in a bigger energy loss in the ice layer at resonant reflection so as to reduce the time delay.

As mentioned in Sec. III, for higher shear velocities (cases 1 and 2) the approximate expression (27) is valid. So the statistical method should give reliable results. For lower shear velocities (cases 3 and 4) using Eq. (27) may produce errors in the resonant region for large numbers of reflections. However, if the PDF function does not concentrate at the resonant thickness, the statistical method may still give reliable results.

V. FRESNEL ZONE RADIUS AT THE SURFACE

A sound ray is not a mathematical line, but rather a finite ray tube. The dimension of the ray tube is related to the Fresnel zone size, which is a function of position along the ray. Therefore, in using the statistical method [Eq. (29)] to estimate the travel-time changes, the PDF of ice draft should be derived after smoothly averaging the ice draft profile with a window whose width equals the Fresnel radius at the surface.

The Fresnel zone radius is given by

$$R_F^2 = (KA)^{-1}, \tag{31}$$

where $K=2\pi/\lambda$, λ is the acoustic wavelength, and A is the phase curvature, which is defined by

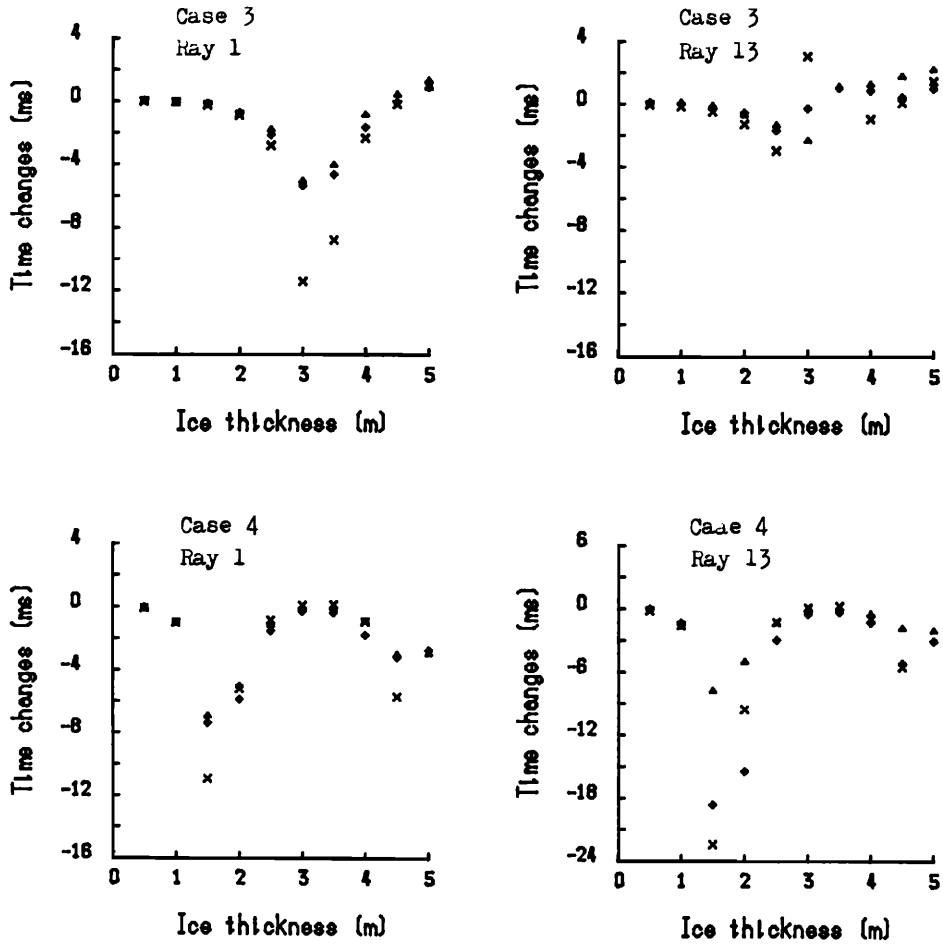

FIG. 8. Calculated travel-time changes of rays 1 and 13 for ice cases 3 and 4 in terms of the three methods. △—method 1, ◇—method 2, ×—method 3.

$$A=\frac{\partial^2}{\partial z^2}S(r,z,R), \tag{32}$$

where S is the acoustic path length and R is the distance between the source and receiver.

In order to estimate the excess acoustic path length associated with the scattered ray at the surface, it is needed to replace the phase curvature A by A_s. The relation between the sensitivities of the eikonal to horizontal (A_s) and to vertical (A) displacements is[19]

$$A_s=A\tan^2\alpha, \tag{33}$$

where α is the grazing angle of the eigenray at the surface. Thus we have

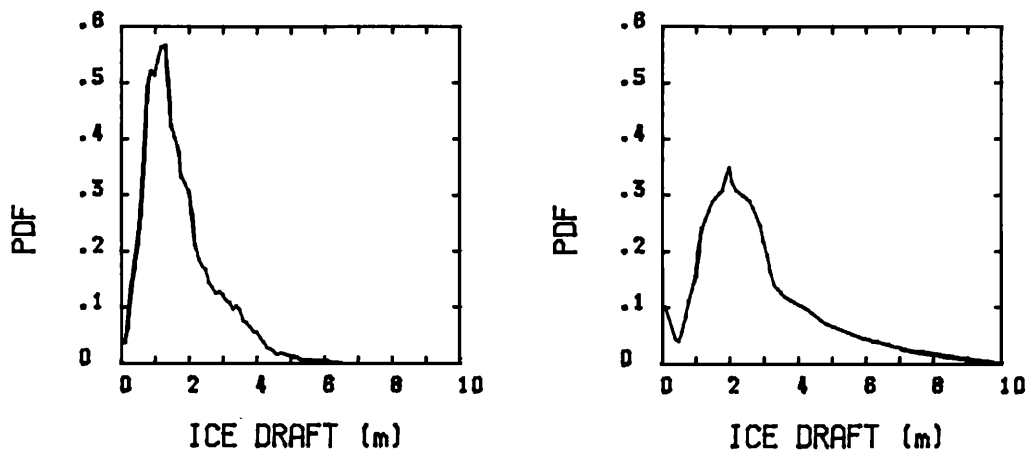

FIG. 9. Probability distribution functions of the ice draft, PDF 1 (left) and PDF 2 (right).

TABLE III. Travel-time changes and standard deviations for rays.

Ray path		1		4		13		16	
		Δt (ms)	σ (ms)	Δt (ms)	σ (ms)	Δt (ms)	σ (ms)	Δt (ms)	σ (ms)
case 1	PDF 1	1.3	0.8	2.5	1.2	1.8	0.7	2.5	0.8
	PDF 2	2.4	1.0	4.8	1.5	3.2	0.8	4.4	1.0
case 2	PDF 1	0.6	0.6	1.2	0.9	1.1	0.6	1.5	0.7
	PDF 2	1.7	1.4	3.3	1.9	2.6	1.1	3.6	1.5
case 3	PDF 1	−0.9	1.1	−1.7	1.6	−0.1	0.3	−0.1	0.4
	PDF 2	−1.0	1.7	−2.0	2.3	0.3	0.8	0.4	1.0
case 4	PDF 1	−3.1	2.1	−6.1	3.0	−7.2	3.8	−10.1	4.5
	PDF 2	−2.9	1.9	−5.7	2.7	−7.2	3.1	−10.0	3.6

$$R_F^s = R_F / \tan \alpha. \tag{34}$$

For Greenland Sea experiment environment the Fresnel zone patch size of the mth reflection point at the surface can be estimated by[19]

$$R_F^s = \sqrt{KRm(N-m)/N^2}/\tan \alpha, \tag{35}$$

where N is the number of surface to surface arcs of the eigenray. The estimated Fresnel zone patch sizes of the first four ray groups for mooring 4–5 range from 700 to 1400 m. Figure 11 shows the PDF derived from the ice draft profile (May 1987 data) by averaging with windows of 500, 1000, and 1500 m, respectively. Note how averaging over increasingly wide windows causes the PDF to become narrower. Table IV gives the travel-time changes calculated in terms of PDF without or with averaging (distance = 1000 m). It is found that the averaging may have considerable effect on the travel-time change for lower shear velocity (case 4) because of the distribution change around the resonant thickness.

VI. SHADOWING EFFECTS

If the along-track slope of a segment of the ice–water interface is greater than the incidence angle of the acoustic beam, that segment is not "seen" by the sound pulse—it falls into a "shadow." When the ice draft d is much smaller than the sound wavelength ($kd \ll 1$), there is no need to consider shadowing effects because of diffraction. However, when d is much bigger than the wavelength ($kd \gg 1$), shadowing should be considered as it will change the PDF of the ice draft. Under the high-frequency approximation, shadowing can be estimated numerically for a certain ice draft profile. When the ice draft is comparable to the sound

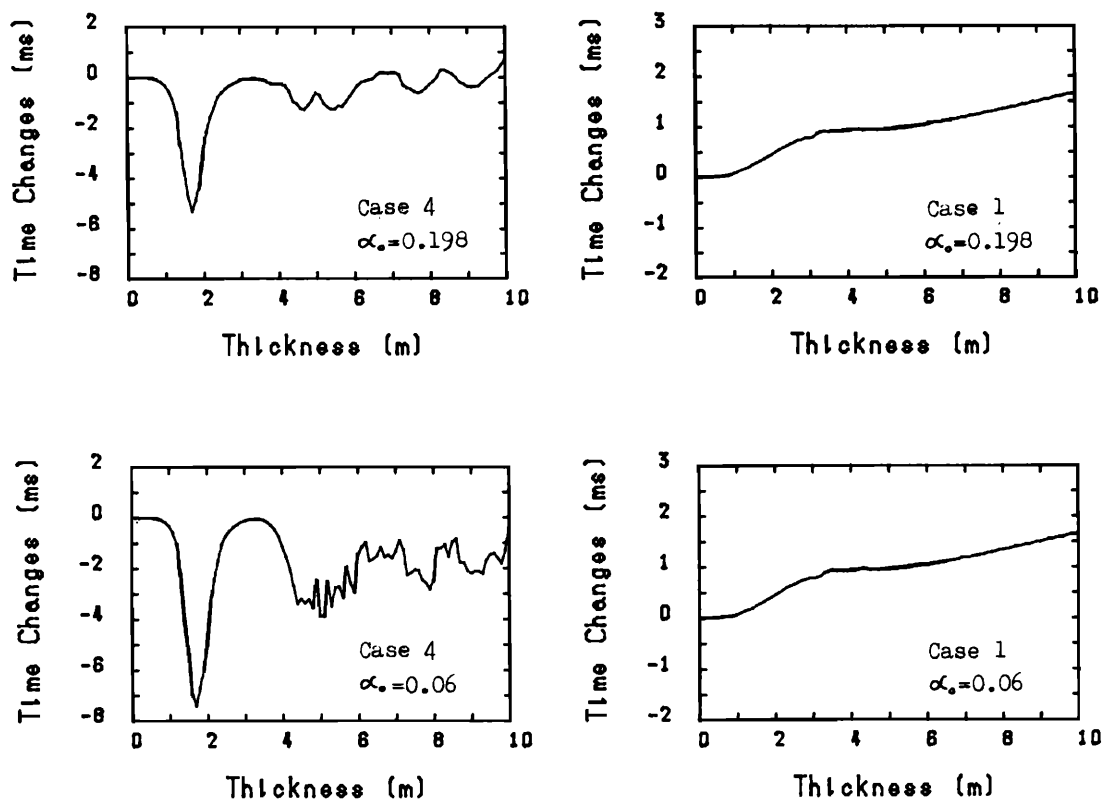

FIG. 10. Calculated $\tau(h)$ at $\theta = 7°$ for ice cases 1 and 4 by using different absorption coefficients, $\alpha_0 = 0.06$ dB/m kHz and 0.198 dB/m kHz.

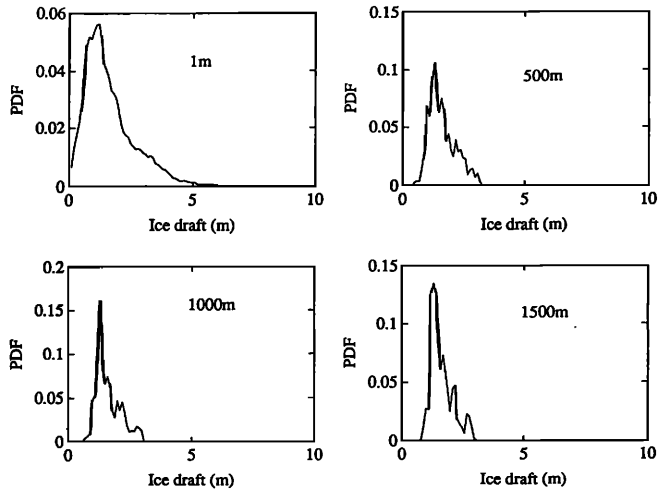

FIG. 11. Effects of Fresnel zone surface patch size averaging on ice during PDF.

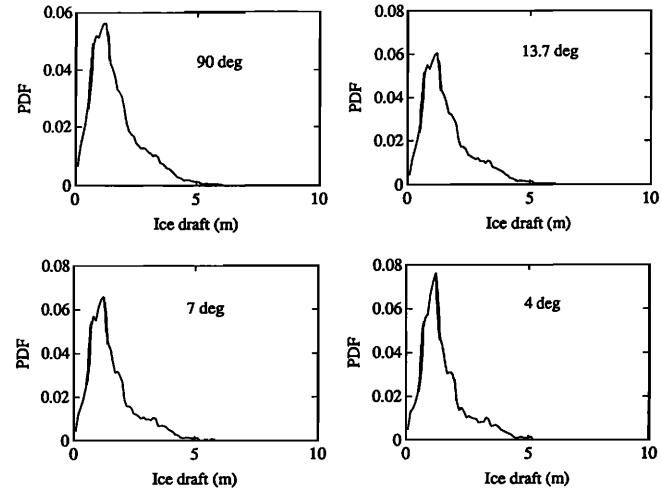

FIG. 12. Effects of shadowing on ice draft PDF.

wavelength, however, there is no easy way to estimate shadowing effects because of partial diffraction. It is expected for the Greenland Sea tomography experiment parameters that the results will be between these two extremes.

As an example, the ice draft profile from the May 1987 data is considered. It is found that 19%, 37%, and 55% of the ice–water interface is shadowed for grazing angles of 13.7°, 7°, and 4°, respectively. The corresponding PDF's are shown in Fig. 12. Table V gives the travel-time changes calculated in terms of PDF without or with considering the shadowing effect. It is found that there are no considerable changes caused by shadowing ($\alpha=13.7°$ and $\alpha=7°$), because, perhaps, the PDF shape changes due to shadowing are small for the particular ice draft profile.

VII. EFFECTS OF TRAVEL-TIME CHANGES ON TOMOGRAPHIC INVERSIONS

As discussed above, the presence of ice will cause travel-time changes on the order of 1 to 10 ms for acoustic eigenrays in a typical Arctic mesoscale tomography experiment (i.e., one with source-receiver separations of several hundred km at most). Since changes of this magnitude are usually considered measurable, the question naturally arises: Do these changes have a significant effect on tomographic inversions for sound speed in the water column?

Since this is somewhat equivalent to asking if the travel-time changes due to ice cover are significant compared with those due to changes in the water column sound speed, a complete answer will require some statements as to the nature of the sound-speed changes we expect to see. This will depend on the nature and objectives of the tomography experiment.

The Greenland Sea tomography experiment (GSP88) was primarily concerned with weekly to seasonal time scales.[7] By examining historical data for the experimental area, we estimated the order of these changes to be perhaps ± 10 m/s at the surface, decreasing exponentially with a scale of approximately 450 m. Near-surface changes can actually be much greater than this but mixed-layers with depths <50 m are almost completely unresolved by the GSP88 array.

We can quantify the ice effects in a simulation by assuming that ice covers a region with a known sound speed. The linearity of the usual forward problem resulting from the assumption of small perturbations about a background sound speed allows us to decompose the resulting inverse estimate of the sound speed perturbation δc into a part due to travel-time changes from variations in the sound speed in the water column δt_{wc}, and a part due to travel-time changes from surface ice effects δt_{ice}.

$$A\delta c=\delta t_{\mathrm{wc}}+\delta t_{\mathrm{ice}}, \tag{36}$$

where A is a linear operator containing the ray path information. For example, if δc is a vector of sound-speed perturbations in a number of discrete depth bins, A is a function depending on the ray path length and sound speed within each bin. Here we will assume $\delta t_{\mathrm{wc}}=0$, and consider the effects of δt_{ice}.

TABLE IV. Travel-time changes (ms) due to Fresnel zone averaging of the PDF.

Path	1		2		13		16	
Average (1000 m)	No	Yes	No	Yes	No	Yes	No	Yes
case 1	1.1	1.1	2.3	2.2	1.5	1.5	2.1	2.1
case 2	0.54	0.38	1.1	0.76	1.0	0.70	1.4	0.98
case 3	−0.84	−0.60	−1.6	−1.2	−0.10	−0.35	−0.14	−0.49
case 4	−2.8	−4.6	−5.6	−9.2	−6.6	−10.9	−9.2	−15.2

TABLE V. Travel-time changes (ms) due to shadowing.

Ray path	1		2		13		16	
Shadowing	No	Yes	No	Yes	No	Yes	No	Yes
case 1	1.1	1.2	2.3	2.3	1.5	1.5	2.1	2.1
case 2	0.54	0.52	1.1	1.0	1.0	0.95	1.4	1.3
case 3	−0.84	−0.78	−1.6	−1.5	−0.10	−0.05	−0.14	−0.07
case 4	−2.8	−2.8	−5.6	−5.6	−6.6	−0.65	−9.2	−9.2

Consider the 4–5 path described previously. Analysis of the GSP88 results shows that we can identify four ray groups for this path with turning depths of approximately 2400, 1400, 900, and 600 m, as well as a final cutoff which is actually a low-numbered modal arrival. Finding a solution to Eq. (36) using the information in the early ray arrivals is fairly standard after assuming path invariance. An exact treatment of the final cutoff requires a modal inverse, but we can form an approximate solution by treating this last arrival as a *zero-degree* launch angle ray. Although path invariance does not really hold for this "ray," this error is compensated somewhat by the smoothing inherent in the inverse.

Since Eq. (36) is, in general, undetermined, there are many possible solutions δc. We can choose an "optimal" solution by making assumptions about the statistical nature of both the travel-time measurements δt and the sound-speed perturbations δc and using the structure of, for example, the Gauss–Markov Theorem. In this case we assumed the travel-time errors for different rays to be independent and to have a variance of 1 ms (actual experimental measurements had errors on the order of 4–10 ms depending on the time of year and other factors). Sound-speed perturbations at depths z_i were modeled by

$$\langle \delta c_i^2 \rangle = \sigma_{ii}^2 = \sigma_0^2 e^{-2z_i/l_d}, \tag{37}$$

with $\sigma_0 = 10$ m/s and a decay scale $l_d = 450$ m determined from examination of historical data. To smooth the inverse we modeled the covariance structure as

$$\langle \delta c_i \delta c_j \rangle = \sigma_{ii}\sigma_{jj} e^{-[(z_i - z_j)/l_z]^2}, \tag{38}$$

where we choose a vertical correlation scale $l_z = 2000$ m. Inverse solutions were fairly insensitive to this choice as long as it was greater than several hundred meters.

In performing the inverse, a travel-time perturbation of zero was chosen for the zero-degree ray. In fact, the shallow-angle energy modeled in this way is affected by surface ice, but the mechanisms for this change may be different than those for the steeper rays discussed here.

Travel-time perturbations were computed using the Fresnel-zone smoothed PDFs for all rays (a subset of these values are given in Table V), and for all 4 cases. The inverse results using only the ice signal are shown in Fig. 13. The advantage of using a linear inverse is that estimates can be made of the errors in the inverse. The inversions for cases 1–3 are generally within these error bounds. This is perhaps not too surprising given that the travel-time perturbations due to the ice are of the same order as the assumed travel-time error.

The inverse for case 4 is surprisingly large. This is because we are close to a resonant point in the ice parameter space, and a large amount of energy is coupled into Lamb waves. Resonance points exist in the other cases, but require much greater ice thicknesses. It is likely that the case 4 shear speeds, which are characteristic of newly formed keels, are grossly low for the average shear speed along the path, which is probably somewhere between cases 1 and 3.

It is important to note that a sound-speed perturbation of 0.1 m/s is roughly equivalent to a temperature change of 0.02 °C. Such a temperature change is generally well below the signals of interest which are of order 0.2–5 °C. Thus the ice does not significantly affect our tomographic estimates for the water column properties in the Greenland Sea.

VIII. SUMMARY

The travel-time changes of acoustic pulses propagating along ray paths, caused by a sea ice cover of uniform thickness, can be estimated rigorously in terms of the generalized ray method [Eq. (12)].

For an ice cover of nonuniform thickness, the travel-time changes can be estimated approximately by adding the time changes due to individual reflections [Eq. (27)]. In this case the statistical method can be used if the probability distribution function of ice thickness is known.

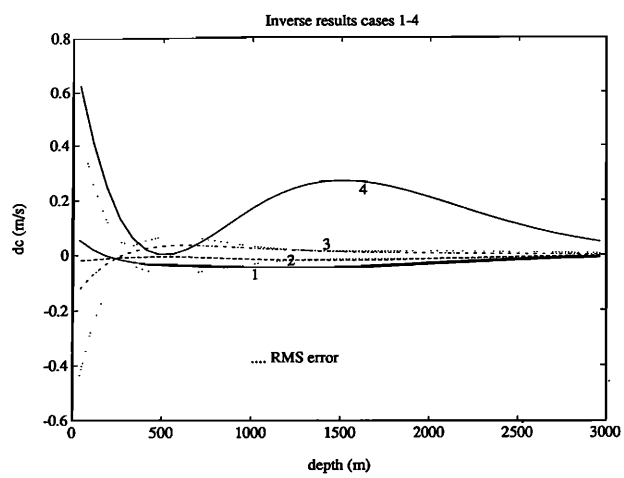

FIG. 13. Error in water column temperature estimate due to ignorance of travel time delays due to ice for cases 1–4. The estimated rms error of the inverse procedure is given by the dotted lines; note that we have a significant ice-related temperature error only for case 4.

For higher shear velocities in ice, which may result in total internal reflection at the ice–water interface, the approximation of Eq. (27) is good and the statistical method can give reliable results. The travel-time changes can be estimated simply from the beam displacement and time delay of the reflection at the central frequency, instead of using the generalized ray method.

For lower shear velocities in the ice, the sound may penetrate into the ice and large errors may be induced by using Eq. (27) at resonant reflection for a large number of reflections. However, the statistical method may still give reliable results if the PDF function does not concentrate at the resonant thickness.

Two effects can modify the PDF one uses in the statistical method: The horizontal averaging of the surface by the Fresnel zone patch size and (geometrical) shadowing by ice roughness. The Fresnel zone patch averaging was seen to have little effect for high ice shear speeds, but could have a pronounced effect for low shear speeds, specifically by peaking the PDF near the resonant thickness for the first resonant mode. Shadowing effects were seen, at least for the Greenland Sea case, not to significantly distort the shape of the PDF, and thus not create significant changes in the ice-induced travel-time disturbance.

From the simulations we found that, in general, the shear velocity and the ice thickness are the two most important ice parameters affecting travel time. Also, sound absorption in ice may be important at resonant reflection.

For the example of the Greenland Sea tomography experiment, the calculated travel-time changes due to an ice cover at the range of 121 km for the first four ray groups are of the order of milliseconds, depending on ice parameters. The travel-time change is approximately proportional to the propagation range (number of reflections) and ice concentration. From inverse results, we see that the errors induced by ice in the water column sound speed (temperature) estimates are of the same order as the measurement noise in the experiment. Only for very low shear speeds, typical of newly formed keels, are the ice-induced errors in the water column sound speed appreciable. As such low shear speeds are not likely to be typical of the entire path (rather, we expect to see $c_s \simeq 1600$ m/s as more typical), we can state that the ice travel-time signals for the Greenland Sea tomography were negligible.

As a penultimate note, we must comment that our ignorance of the ice PDF (which varies greatly, both temporally and spatially) and the ice material parameters (which also vary within time and space) are the greatest limitations to our knowing the *exact* travel-time errors induced by the ice. However, by considering both a wide range of ice parameters, we have shown that, given reasonable assumptions of ice characteristics in the Greenland Sea, ice effects on travel time should be negligible.

Finally, we should note that relevance of our work, or more precisely the lack of it, to a proposed scheme by P. Mikhalevsky, R. Muench, and F. DiNapoli to monitor global warming effects on the Arctic ice pack by using an acoustic path across the Arctic basin.[20,21] Due to their planned use of 30-Hz sound, for which the acoustic wavelength is much greater than the ice thickness, they are in a much different scattering regime than the one we have explored here. Also, they are planning a cw experiment, so that one must deal with phase resolution issues, which are somewhat different than the travel-time related issues we addressed. And finally, they are dealing with a long-range transmission across a much less dynamic ocean (the Arctic), whereas we were looking at an order of magnitude shorter path across a much more dynamic region (the Greenland Sea). However, in terms of the *amplitude* of the scattering one might see, some of our recent Greenland Sea results might have some relevance. These results are currently in preparation for publication.[22,23]

ACKNOWLEDGMENTS

The authors would like to acknowledge the following people for their contributions to this work. Dr. Robert Shuchman of the Environmental Research Institute of Michigan and Dr. Ola Johannessen of the Nansen Environmental and Remote Sensing Center of Bergen, Norway contributed the satellite information on the ice cover. Dr. Peter Worcester of the Scripps Institute of Oceanography was a co-investigator for the Greenland Sea Tomography Experiment and provided useful comments. Dr. Peter Mikhalevsky of Science Applications International Corporation provided the material concerning the use of acoustics to monitor the Arctic ice peak. Mr. Arthur Newhall of WHOI provided programming assistance, and Ms. Shirley Bowman of WHOI typed the manuscript.

This work was supported jointly by NSF (SIO) and ONR (WHOI) under Grant Nos. N00014-91-J-1139 and N00014-92-J-1291. This is WHOI contribution number 8111.

[1] W. H. Munk and C. Wunsch, "Ocean acoustic tomography in a scheme for large scale monitoring," Deep-Sea Res. **26**, 123–161 (1979).

[2] B. D. Cornuelle, "Tomographic maps of the ocean mesoscale, 1: Pure acoustics," J. Phys. Oceanogr. **15**, 133–152 (1985).

[3] F. Gaillard and B. D. Cornuelle, "Improvement of tomographic maps by using surface reflected rays," J. Phys. Oceanogr. **17**, 1458–1467 (1987).

[4] D. B. Chester, P. Malanotte-Rizzoli, and H. DeFerrari, "Acoustic tomography in the Straits of Florida," J. Geophys. Res. **96**, 7023–7048 (1991).

[5] P. F. Worcester, B. Dushaw, and B. Howe, "Gyre Scale Reciprocal Acoustic Transmission," in *Ocean Variability and Acoustic Propagation*, edited by J. Potter and A. Warn-Varnas (1991).

[6] J. F. Lynch, J. H. Miller, and C. S. Chiu, "Phase and travel time variability of adiabatic acoustic normal modes due to scattering from a rough surface, with applications to propagation in shallow water and high-latitude regions," J. Acoust. Soc. Am. **85**, 83–89 (1989).

[7] P. F. Worcester, "Ocean acoustic tomography in the Greenland Sea," Geophys. Res. Lett. (1992) (in press).

[8] J. J. Romm, "Application of normal mode analysis to ocean acoustic tomography," Ph.D. thesis, MIT, Cambridge, MA (1987).

[9] G. Jin, and P. Wadhams, "Travel time changes in a tomography array caused by a sea-ice cover," Prog. Oceanogr. **22**, 249–275 (1989).

[10] H. Weinberg, "Application of ray theory to acoustic propagation in horizontally stratified oceans," J. Acoust. Soc. Am. **58**, 97–109 (1975).

[11] D. Wang, and E. C. Shang, *Underwater Acoustics* (Beijing, 1981).

[12] L. M. Brekhovskikh, *Waves in Layered Media* (Academic, New York, 1980).

[13] D. F. McCammon and S. T. McDaniel, "The influence of the physical properties of ice on reflectivity," J. Acoust. Soc. Am. **77**, 499–507 (1985).

[14] K. Hunkins, "Seismic studies of sea ice," J. Geophys. Res. **65**, 3459–3476 (1960).
[15] P. L. Gruber, "An experimental study of the coherent under-ice reflectivity of sound in the Greenland Sea marginal ice zone," Ph.D. thesis, University of Miami (1987).
[16] O. I. Diachok, "Acoustics of sea ice ridges," Proceedings of the 12th International Congress on Acoustics (1986).
[17] P. Wadhams, "Sea-ice thickness distribution in the Trans Polar Drift Stream," Rapp. P. V. Reun. Cons. Int. Explor. Mer **188**, 59–65 (1989).
[18] P. Wadhams, "Sea ice thickness distribution in the Greenland Sea and Eurasian Basin, May 1987," J. Geophys. Res. **97**, 5331–5348 (1992).
[19] S. Frankenthal, "The reflection of radiation from randomly irregular surfaces," J. Acoust. Soc. Am. **81**, 1377–1384 (1987).
[20] P. N. Mikhalevsky, R. D. Muench, and F. R. DiNapoli, "Arctic Ocean warming; Can we measure it acoustically," paper presented at 2nd Meeting of the Oceanographic Society, St. Petersburg, Florida, March 1991.
[21] P. N. Mikhalevsky, R. D. Muench, and F. R. DiNapoli, "Acoustics measurements of Arctic Ocean warming," NSF proposal (March 1991).
[22] P. J. Sutton, P. F. Worcester, G. Masters, B. D. Cornuelle, and J. F. Lynch, "Ocean mixing layers and acoustic pulse propagation in the Greenland Sea," submitted to J. Acoust. Soc. Am. (1992).
[23] G. Jin, J. F. Lynch, R. Pawlowicz, and P. F. Worcester, "Acoustic scattering losses in the Greenland Sea marginal ice zone," J. Acoust. Soc. Am. (to be published).